Applied Surface Science 592 (2022) 153315

Contents lists available at ScienceDirect

Applied Surface Science

journal homepage: www.elsevier.com/locate/apsusc

Full Length Article

The role of fluence in determining the response of thin molybdenum films to ultrashort laser irradiation; from laser-induced crystallization to ablation via photomechanical ablation and nanostructure formation

Ayesha Sharif [a,b,*], Nazar Farid [a], Mingqing Wang [c], Kwang-Leong Choy [c], Gerard M. O'Connor [a,b]

[a] National Centre for Laser Applications (NCLA), School of Physics, National University of Ireland Galway, Galway, Ireland
[b] I-Form, the SFI Research Centre for Advanced Manufacturing, National Centre for Laser Applications (NCLA), School of Physics, National University of Ireland Galway, Galway, Ireland
[c] Institute for Materials Discovery, University College London, London, UK

ARTICLE INFO

Keywords:
Molybdenum
Ultrashort pulses
Laser-induced crystallization
Laser-induced ablation
Stress assisted ablation
Nanostructures

ABSTRACT

The selective processing of Mo at low temperatures is challenging, especially in advanced manufacturing on flexible and heat-sensitive substrate due to its higher melting temperature. The key role of fluence in determining the response of thin Mo films to ultrashort laser irradiation is considered in this study. At low fluences, the electrical properties of Mo are enhanced by a localized laser-induced crystallization mechanism; the electrical mobility of Mo is increased and the contact resistance between Mo-Si interface is reduced. At higher fluences, selective patterning of Mo proceeds without impacting the Si layer and the threshold fluence for ablation increases with the film thickness of Mo. Two fluence dependent ablation mechanisms are observed depending on the Mo film thickness. For thin films of thicknesses 20 nm and 40 nm, selective ablation proceeds only by a photothermal interaction. For 60 nm and 80 nm thick films, selective ablation proceeds by both photomechanical and photothermal interactions at two-separate higher fluence regimes, respectively. Interestingly, between these two ablation regimes, a non-ablative nanostructuring regime occurs. The study provides a concise overview of the process window for implementing the laser-induced modifications to Mo layers with minimal impact to the substrate using single wavelength ultrashort pulse laser.

1. Introduction

Molybdenum (Mo) has attractive properties such as high melting temperature, high thermal and electrical conductivity, excellent corrosion resistance and low coefficient of thermal expansion. Such unique properties make Mo a potential candidate for its use in high temperature electrical and electronic device applications [1]. Due to its higher reflectivity over a broad range of electromagnetic spectrum and higher melting temperature, Mo has also been used as a first mirror material in nuclear fusion devices such as EAST and HL-2A tokamaks and also considered as a candidate mirror material in ITER tokamak [2]. In thin film based electronic devices, Mo coatings are the crucial components of thin film transistors in liquid crystal display technology (TFT-LCD), where the low thermal diffusion constant of Mo helps to prevent the device failure in a TFT-LCD [3,4]. Mo films are extensively used as a source/drain electrode material and also for gate metallization in TFTs [5]. Moreover, Mo is a good ohmic contact material and serves as a promising electrode material due to its lower resistivity [6,7].

The emerging new generation of foldable, rollable, and stretchable display technology which is built around organic light emitting diodes (OLEDs) have attracted attention globally. Foldable smart screens and wearable devices are examples of this newly adaptive innovative technology [8]. The efforts to develop foldable displays continue to improve and require the deposition of the demanding working materials such as Mo and indium tin oxide (ITO) on flexible heat-sensitive substrates. This is challenging as Mo has a high melting temperature and cannot be easily processed or crystallized at low temperatures. The need for higher temperature also limits the use of heat-sensitive polymers as substrate. Therefore, the conventional deposition methods are not suitable to facilitate the requirement of enhanced electrical properties, performed

* Corresponding author.
E-mail address: a.sharif1@nuigalway.ie (A. Sharif).

https://doi.org/10.1016/j.apsusc.2022.153315
Received 18 February 2022; Received in revised form 2 April 2022; Accepted 3 April 2022
Available online 5 April 2022

using RF or DC magnetron sputtering and e-beam evaporation followed by a post process annealing step [9–11]. In such cases the thermal annealing is not localized, and it could lead to melting and damaging of the nearby components.

Laser technology provides a reconfigurable and precise solution to such problems in a highly selective manner without affecting the nearby components and underlying layers [12]. Selective ablation and patterning of Mo thin films from transparent and multilayered structures have been studied extensively using nanosecond [13,14], picosecond [15], and femtosecond [16,17] laser pulses. The experimental and theoretical studies reveal that a less thermal damage was observed at ultrashort laser pulse duration. Ultrashort lasers with higher repetition rates are promising in selective ablation, patterning, cutting, drilling and crystallization of metals, polymers, dielectrics, ceramics and thin films [12,18–22] as the duration of the pulses is much shorter than the duration of electron–lattice relaxation processes [23]. In ultrashort laser-metal interactions, upon absorbing the laser energy; electrons heat up to thousands of Kelvins within few femtoseconds (*fs*) due to the small heat capacity of electrons. The lattice temperature remains almost unchanged and is considered as cold during the absorption process. These excited electrons then thermalize and transfer their energies to the lattice through electron-phonon coupling. This two-step non-equilibrium energy transfer has been extensively described by a two-temperature model (TTM) [24,25]. In this study, we utilize this two-temperature nature of ultrashort laser pulse interactions to investigate the response of a thin molybdenum film. We demonstrate how the crystallinity, and the electrical properties are enhanced after scanning with overlapped femtosecond laser pulses in the visible region of the electromagnetic spectrum. Upon increasing the fluence, two fluence dependent ablation regimes are obtained depending on the film thickness. Between these two fluence regimes, a practically non-ablative nanostructuring regime is encountered. The green femtosecond laser wavelength was able to probe these different ablation mechanisms which were not clearly resolved in the previous study carried out with IR femtosecond laser pulses on Mo in a multilayered molybdenum-aluminum-molybdenum (MAM) system, where it was proposed that the electron emission played a crucial role in the photomechanical ablation of Mo films from the aluminum layer [26]. The process parameter window, defined by the laser fluence and thin film thicknesses, offers important insight to the potential for further precision tuning of ultrashort laser metal interactions.

2. Materials and methods

Commercially available Mo thin film samples of four different thicknesses i.e., 20 nm, 40 nm, 60 nm, and 80 nm are used in current study. Fig. 1 presents a schematic showing the structure and fabrication steps of the Mo sample set. Mo thin films are fabricated using magnetron sputtering onto a 50 nm amorphous silicon (a-Si), which is itself deposited on a dielectric (SiO_2) layer of 300 nm thickness using a chemical vapor deposition (CVD) method. The SiO_2 layer is coated on 0.4 mm glass substrate using CVD deposition process.

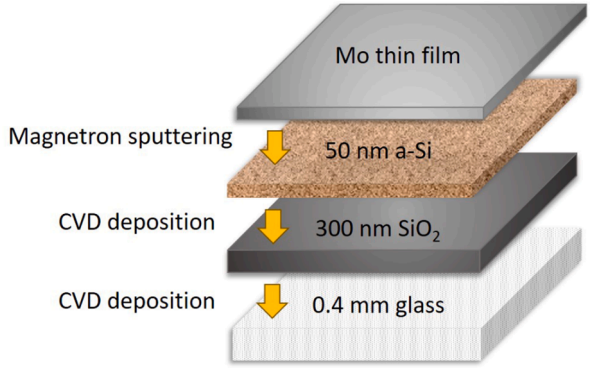

Fig. 1. Schematic diagram exhibiting the composition and coating methodology of Mo thin films samples.

To explore laser-induced effects and corresponding laser-induced crystallization and ablation mechanisms in various Mo thin films thicknesses, a femtosecond laser system (s-Pulse HP Amplitude systems) of 515 nm wavelength is used as an irradiation source. The laser pulse duration is 500 *fs*, capable of operating from single pulse to 300 kHz repetition rate. A three-dimensional computer-controlled stage (Aerotech 3200, Aerotech Inc) is integrated with the system to enable precision control of sample positioning with sub-micron level accuracy. The laser is focused with a telecentric f-theta lens of 100 mm focal length and 0.014 numerical aperture. A galvanometer based XY beam scanning system (SCANLAB, hurrySCAN® II) is used to control the pulse to pulse overlap on the sample. The polarization state of the laser is changed with a half-wave plate placed before the scanning system. An optical microscope and scanning electron microscope, SEM (Hitachi S-4700) is utilized for laser crater depth and surface morphology analysis. A simple voltage source measuring unit (Ossila X200) is used to obtain the online measurement of current flow before, during and after laser scanning of Mo film. To observe the effects of laser fluence on charge carrier mobility and concentration, the Hall measurements were performed before and after laser irradiation using an Ecopia Hall Effect Measurement system (HMS-3000).

3. Results

The Gaussian shaped beam spot diameter $(2\omega_o)$ at the focused position $(1/e^2)$ and the ablation threshold was calculated experimentally using Liu's method [27]. The calculated ω_o for 515 nm laser wavelength is 20.84 μm ± 0.09 μm. The ablation threshold laser fluence is the fluence at which Mo film starts to ablate as observed by the SEM. It is useful to consider the reflection and transmission of the green wavelength for Mo [28] as this provides the actual fluence that is absorbed by the material. The absorbed fluence is calculated by subtracting a total factor of 0.69 (transmission + reflection) from the applied fluence values. Therefore, it is the absorbed threshold fluence that is used throughout the text.

Fig. 2 presents the dependence of a single pulse ablation threshold as a function of film thickness, measured for 20 nm, 40 nm, 60 nm, and 80 nm thick Mo films, respectively. Two ablation regimes are observed for higher film thicknesses at higher fluences as shown in Fig. 2. These

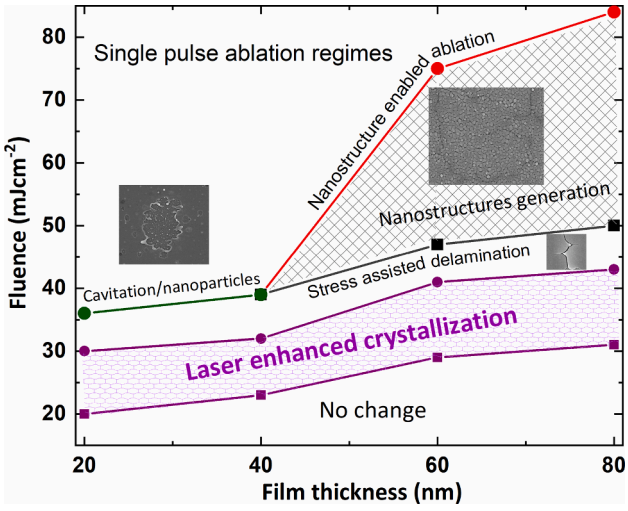

Fig. 2. Laser fluence regimes for crystallization and ablation of 20 nm, 40 nm, 60 nm, and 80 nm thick Mo films, respectively. The insets are the SEM micrographs of the laser ablated surfaces.

regimes can be classified in terms of the laser fluence, as: (I) low fluence ablation regime and: (II) higher fluence ablation regime, respectively. It is evident that the ablation threshold fluence increases with increasing film thickness for each regime. A nanostructuring regime on thicker films is evident between the two ablative fluence regimes. A crystallization region is found for all film thicknesses on further reducing the fluence below the ablation threshold revealing that a change in grain structure occurs at very low fluences as shown in Fig. 2. No apparent effects (e.g., enhanced grain sizes, damage/ablation) are observed below the crystallization regime. We will discuss the response of the Mo film when laser interacts with the material starting from the low fluence (crystallization regime) to high fluence (ablative regimes), respectively.

3.1. Crystallization regime

The precise control of laser parameters in an optimized fluence range below the onset of damage can enable a solid-state crystallization process in Mo thin films without damaging the underlying a-Si layer. To explore the effect of laser irradiation on the evolution of polycrystalline grain microstructure, the Mo films were scanned with 180 mms^{-1} scan speed at 100 kHz laser repetition rate which provides 95% pulse overlapping with 25 spots per area (SPA). The Mo films were scanned in such a way that laser scans a whole area of 10 mm × 10 mm with 7 μm hatching to obtain maximum uniform exposure. Fig. 3 reveals the comparison of surface morphology of 60 nm and 80 nm thick Mo films before and after the laser scanning. The SEM micrographs of as deposited Mo films (Fig. 3a & c) exhibit that the films are initially composed of irregularly shaped islands with wider gaps consisting of nanosized particles of size circa. 18 nm in 60 nm thick Mo film and circa. 20 nm in 80 nm thick Mo films, respectively. In 60 nm thick Mo film at a fluence of 18 $mJcm^{-2}$, the randomly oriented particles transform into well-aligned dense particles of average size 36 nm ± 3 nm (Fig. 3b); the shape of the particles changes to be more spherical with some degree of minor vertical growth superimposed on the film structure. Similarly, the average particle size of 80 nm thick Mo film increases from 20 nm to 42 nm ± 5 nm after scanning at 20 $mJcm^{-2}$ fluence. Careful analysis of the SEM images shown in Fig. 3 suggests that the grain growth occurred locally due to a solid-state diffusion process.

3.1.1. In-situ measurements

While SEM micrographs provide clear evidence of variations in the grain size as a result of laser-induced crystallization, it is interesting to perform an *in-situ* electrical measurement that can demonstrate the change in the electrical conduction as laser starts to scan the Mo thin film sample. To perform such *in-situ* measurement, a simple electrical circuit is made as shown in Fig. 4a. Two electrical contacts are fabricated on 60 nm thick Mo film which are connected to a voltage source meter (Ossila). The measured electrical signal is plotted in Fig. 4b which describes the electrical behavior of the sample before, during and after the laser exposure. For the unexposed film (no laser), the current is constant (circa. 91 mA) with negligible variations. When laser turns ON and starts scanning the region between the two probes on the sample, the current rises and reaches to a maximum of 95.5 mA; this value of current is maintained when the laser scanning is OFF. This *in-situ* measurement provides further evidence of femtosecond laser annealing effect on the electrically isolated thin film structure.

3.1.2. Contact resistance

Contact resistance between layers plays an important role when fabricating thin films of different materials as it defines the nature of adhesion and current flow between the different interfaces. High contact resistance across the interface can significantly degrade the device performance. The contact resistance is greatly affected by the temperature, and it is observed that laser-induced crystallinity in the upper metal layer can significantly reduce the contact resistance between the Mo-Si interface. To investigate the effect of laser-induced crystallinity on contact resistance, a simple setup was prepared as shown in Fig. 5. A region of Mo film is isolated (2 mm diameter), and a small region (0.8 mm) is selectively ablated at low fluence to remove the upper Mo film from the a-Si layer. This provides two separate Mo and a-Si surfaces on

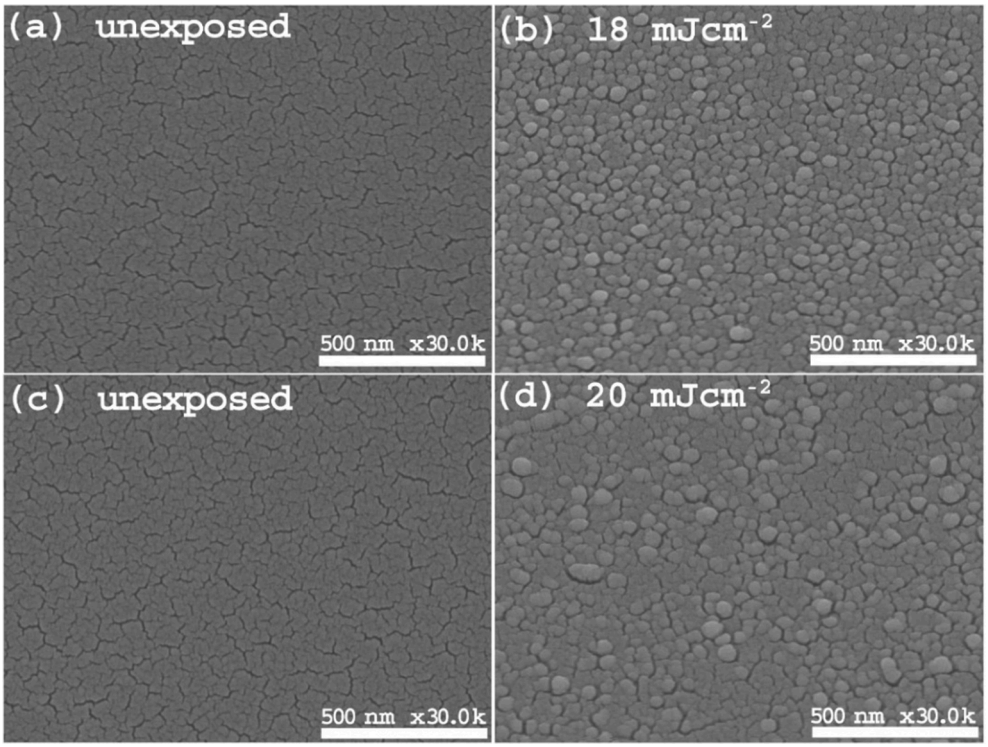

Fig. 3. SEM images revealing the variations in surface morphology of 60 nm (a & b) and 80 nm (c & d) thick Mo films before and after femtosecond laser annealing using 95% pulse to pulse overlapping.

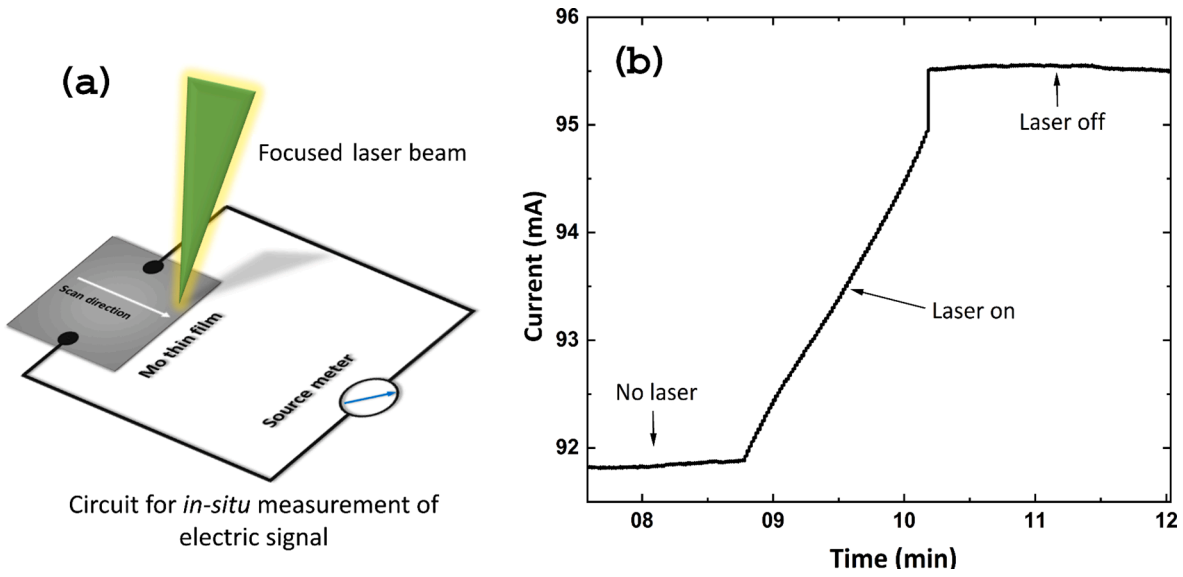

Fig. 4. (a) A simple circuit used for in-situ measurement of the electrical signal, and (b) shows the variation in current flow versus time before, during and after the laser scanning of 60 nm thick Mo film.

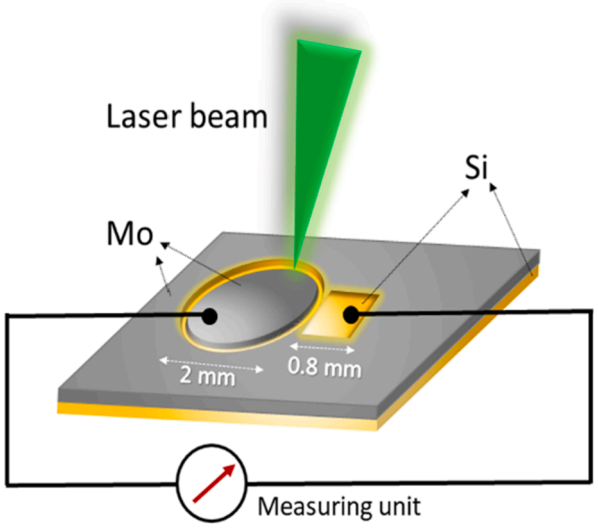

Fig. 5. Schematic showing the simple setup prepared to measure the contact resistance of Mo-Si interface before and after laser exposure.

which electrical contacts can be made, connected to a source meter. The contact resistance of Mo-Si interface is measured before and after laser scanning of the 60 nm thick Mo film. After the laser crystallization, contact resistance of Mo-Si interface decreased from 6.59×10^8 Ω to 3.2×10^8 Ω. This measurement reveals that the laser crystallization not only increases the grain size and improves the electrical properties but also leads to a reduced contact resistance of the Mo-Si interface. It should be noted that the reduced interface contact resistance is due to the crystallization of upper Mo film only which is scanned at fluence lower than the ablation threshold of Mo film. The lower a-Si substrate layer was unaffected during this process which is confirmed through a simple qualitative etching test using adhesive sticky tape where it was not possible to remove the Mo film due to strong adhesion of the film with the substrate.

3.1.3. Hall measurements

Laser annealing of thin films not only improves the crystal structure, but it also improves the electrical properties. To observe the effect of large area crystallization on charge carrier mobility and concentration, Hall measurements are performed on unexposed, and laser exposed 20 nm, 40 nm, 60 nm, and 80 nm thick Mo films. The variation in mobility and carrier concentrations are graphically presented in Fig. 6. The effect of crystallization on the charge carrier mobility is of prime importance since the carrier mobility is sensitive to thin film structure such as crystallinity, grain orientation, grain boundaries and the grain size. The overall mobility of Mo films increases with increasing film thickness when compared to untreated films (Fig. 6a). The mobility of as-deposited Mo film of thickness 20 nm improves by 29% after laser annealing. Similarly, the mobility increases by 33% for the 40 nm film, 12% for 60 nm film and 37% for 80 nm thick Mo film. Whereas, in comparison, we observed smaller variations in carrier concentration (Fig. 6b) and the carrier concentration slightly decreases after laser annealing in all film thicknesses except in the 80 nm film, where both, mobility and carrier concentration are improved after laser treatment. The carrier concentration reduces by −10% in 20 nm Mo films, −12% in 40 nm films and −1.4% in 60 nm thick Mo films after laser annealing, respectively. However, the charge carrier concentration is increased by + 4.6% in laser treated 80 nm thick Mo films. It can be concluded that the laser annealing of Mo thin films leads to an enhancement in the film's crystallinity and average grain size, and reducing the number of grain boundaries, which further leads to higher mobility. Whereas the effect of laser annealing on carrier concentration is less significant with minor variations in the values, especially in thicker films. The laser exposure of Mo thin films in the air has much less influence on the surface and bulk defect densities. During Laser exposure in the air, a small number of surface defects might be generated, which leads to the minor decrease of carrier concentration in thin Mo films. As the thickness of Mo film increases, the effect of surface defects becomes less influenced on the carrier concentration, while the enhanced crystallization results in a minor decrease of bulk defects and a minor increase of carrier concentration. The measured values of mobility and carrier concentration before and after laser annealing are provided in Table 1.

3.2. Single pulse laser-induced ablation regimes

Laser scanning of Mo films using low fluences (below the ablation threshold) results in an enhanced crystallization with the improvements in the grain microstructures. Increasing the fluence above the crystallization threshold results in the transition of crystallization regime into the ablation regime which strongly depends on the film thickness. In

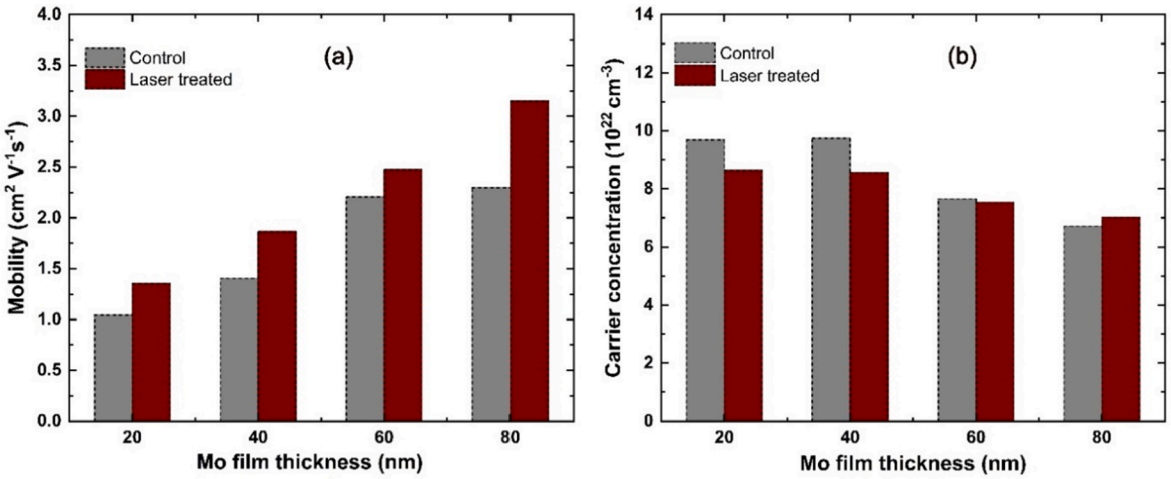

Fig. 6. The variation in (a) mobility and (b) charge carrier concentration of 20 nm, 40 nm, 60 nm, and 80 nm thick Mo films before and after laser annealing.

Table 1
The variations in the electrical properties of Mo thin films before and after femtoseconds laser annealing.

Film thickness (nm)	Mobility ($cm^2 V^{-1}s^{-1}$)		Carrier concentration (cm^{-3})	
	Before	***After***	***Before***	***After***
20	1.05	1.35	9.68×10^{22}	8.63×10^{22}
40	1.40	1.86	9.73×10^{22}	8.56×10^{22}
60	2.20	2.47	7.65×10^{22}	7.54×10^{22}
80	2.30	3.15	6.71×10^{22}	7.02×10^{22}

Fig. 2, we presented two ablation regimes categorized as (I) low fluence regime, and (II) high fluence regime. These regimes are discussed in detail using SEM micrographs in the section below.

Regime I- Low fluence ablation: This ablation regime is observed in all film thicknesses but the type of ablation mechanism changes with varying film thickness. Therefore, thickness is an important factor that defines the mode of ablation. The SEM micrographs in Fig. 7 reveal the different ablation behavior of 20 nm, 40 nm, 60 nm and 80 thick Mo films, respectively. Considering the lower thicknesses such as 20 nm and 40 nm, a partial ablation (Figs. 7-a1 & 7-b1) and complete ablation (Figs. 7-a2 & 7-b2)) is observed at two different laser fluences. At the lower fluence, the film starts to damage with the formation of craters of average size 1.15 μm ± 0.17 μm for 20 nm film and 0.35 μm ± 0.03 μm in 40 nm thin Mo film respectively, where the absorbed laser energy resulted in the formation of trapped cavitation bubbles and the ejection of nanoparticles on film surface. A very modest increase in laser fluence results in a dramatic change from many localized craters to a single large-scale crater (6.56 μm in 20 nm film and 5.73 μm in 40 nm thin Mo film) formation and the film is completely removed from the center of the crater (Fig. 7-a2 & 7-b2). At this stage, the average size of small, localized craters changes to 0.34 μm ± 0.05 μm in 20 nm thin film (Fig. 7-a2) and 0.84 μm ± 0.04 μm in 40 nm thin Mo film (Fig. 7-b2), respectively. The ablation behavior does not vary in low film thicknesses with varying laser fluence, only the density and size of laser crater formation increases with slight increase in the fluence with nanostructures formation. Therefore, we consider that the ablation in low fluence regime occurs only due to a single ablation mechanism through a nanostructure mediated ablation in 20 nm and 40 nm thin Mo films.

For high thickness film such as 60 nm and 80 nm thickness, the ablation mechanism changes from nanostructure enabled ablation to a non-thermal stress assisted delamination as observed in low fluence regime (Fig. 7-c1 & 7-d1). The coalescence of smaller grains into larger grain is also evident in the low fluence regime in 60 nm and 80 nm thick Mo film but the crystallization is accompanied with the surface cracking. The formation of tensile stresses and the grain agglomeration to form larger grains cause the film delamination due to surface cracking. The stress assisted ablation occurs at 47 $mJcm^{-2}$ in 60 nm film and at 50 $mJcm^{-2}$ in 80 nm thick Mo film, respectively. The mechanism of stress generation and corresponding laser ablation is discussed in detail in Section 3.3.1 considering 80 nm thick Mo films.

Regime II- Higher fluence regime: This regime is manifested in thicker films such as 60 nm and 80 nm thick Mo films. When the fluence is increased further, surface cracking become less evident with a transition of stress assisted ablation to nanostructure facilitated ablation behavior. This transition of ablation mechanisms is only observed in 60 nm and 80 nm thick film. On increasing the laser fluence, the formation of nano jets and nanostructures is observed with reduced surface cracking as represented by patterned area in Fig. 2. A complete ablation of 60 nm Mo film is obtained at 75 $mJcm^{-2}$ (Fig. 7-c2). In 80 nm thickness, Fig. 7-d2 exhibit partial ablation due to nanostructures formation associated with the material ablation via nanoparticle emission from the center at 79 $mJcm^{-2}$. The complete removal of 80 nm thick film is obtained at 84 $mJcm^{-2}$.

3.3. Description of ablation mechanism in ultrashort laser material interaction

Ultrashort laser ablation of metals is an intricate process and requires the understanding of physics behind the interaction of an ultrashort laser pulse and the corresponding response of the material. We observed two different ablation regimes as presented by Fig. 2 and the supporting SEM images as shown in Fig. 7. To study the dependence of the single pulse laser-induced ablation mechanisms on the laser fluence, the 80 nm thick Mo film is irradiated from low to a higher laser fluence range as shown in Fig. 8. The transition of one ablation mechanism into the other is discussed below.

3.3.1. Stress assisted ablation-low fluence regime

Fig. 8 presents a detailed study of single pulse laser fluence on film morphology and ablation behavior for 80 nm thick Mo film. The first column (Fig. 8-a1 to 8-e1) shows the laser irradiated region at varied laser fluences while the second (Fig. 8-a2 to 8-e2) and third column (Fig. 8-a3 to 8-e3) presents the high-resolution images. At a low fluence of 32 $mJcm^{-2}$, there is no damage, but the morphology of the film starts to change into well-defined spherically shaped closed particles of average estimated diameter of 11 nm ± 3 nm (Fig. 8-a1 to 8-a3). A slight cracking is observed which is only visible at higher resolution (Fig. 8-a3). Upon increasing the fluence to 43 $mJcm^{-2}$, the nano cracks are more evident and become wider with a gap of 10 nm ± 2 nm (Fig. 8-b1

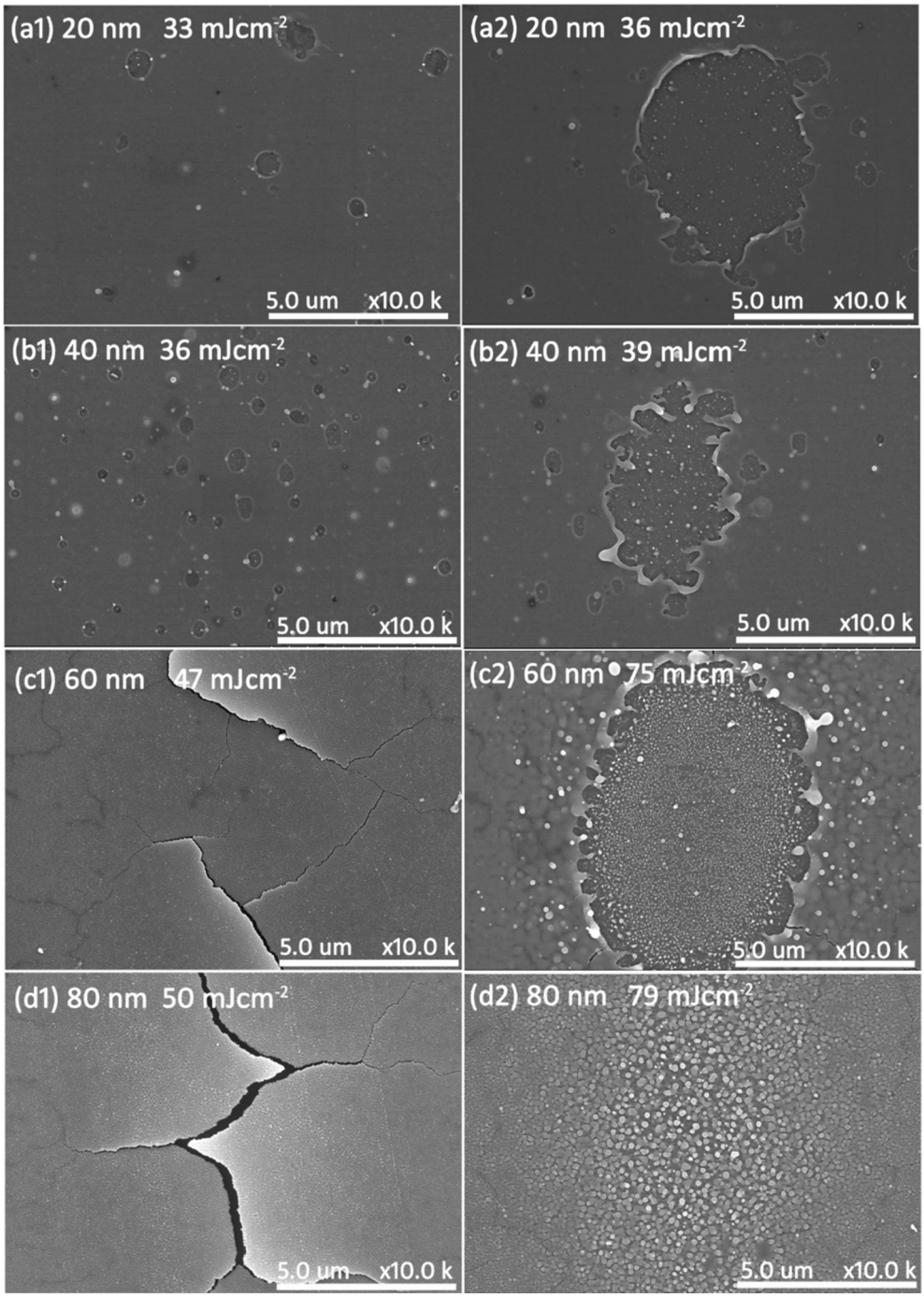

Fig. 7. SEM micrographs revealing the thickness dependent ablation morphologies at a single pulse in 20 nm, 40 nm, 60 nm, and 80 nm thick Mo films, respectively.

to 8-b3). It should be noted that there is no apparent melting of the Mo film, neither there is any damage visible on the underlying substrate layer. The density and size of spherically shaped particles increases to 14 nm ± 2 nm due to the agglomeration of smaller particles and the enhancement in the grain/particle size is more pronounced at this stage (Fig. 8-b3). The films start to delaminate with micro cracks due to expansion of laser heated volume in the film when the fluence is raised to 50 mJcm^{-2} (Fig. 8-c1 to 8-c3). Here we marked this fluence as a threshold for stress generation leading to fracture and delamination in the low fluence regime. It is noticeable that the absorbed fluence not only triggers the distortion in the film with increasing fluence, but also crystallizes the metal film as evident from the improvements in the average particle size (Fig. 8-c3). The particles are no longer spherical in shape instead they are elongated with an elongation length of circa. 38 nm. No apparent melting of the Mo film or the underlying substrate is observed in SEM images (Fig. 8 (a1-c3)).

In ultrashort laser material interaction, the rapid absorption of laser energy by free electrons in metals within the optical penetration depth not only leads to a sharp temperature rise in the irradiated zone but may also result in the formation of the compressive stresses as we observed in Figures (8-a3, 8-b3 & 8-c3). The delamination of 80 nm thick Mo film at 50 mJcm^{-2} can be explained by stress assisted ablation mechanism. To fulfil the criteria for stress assisted ablation, two conditions must be fulfilled; one is the thermal confinement and second is the stress confinement [18,29]. For thermal confinement, the maximum laser energy must be absorbed from laser pulse to the irradiated region with

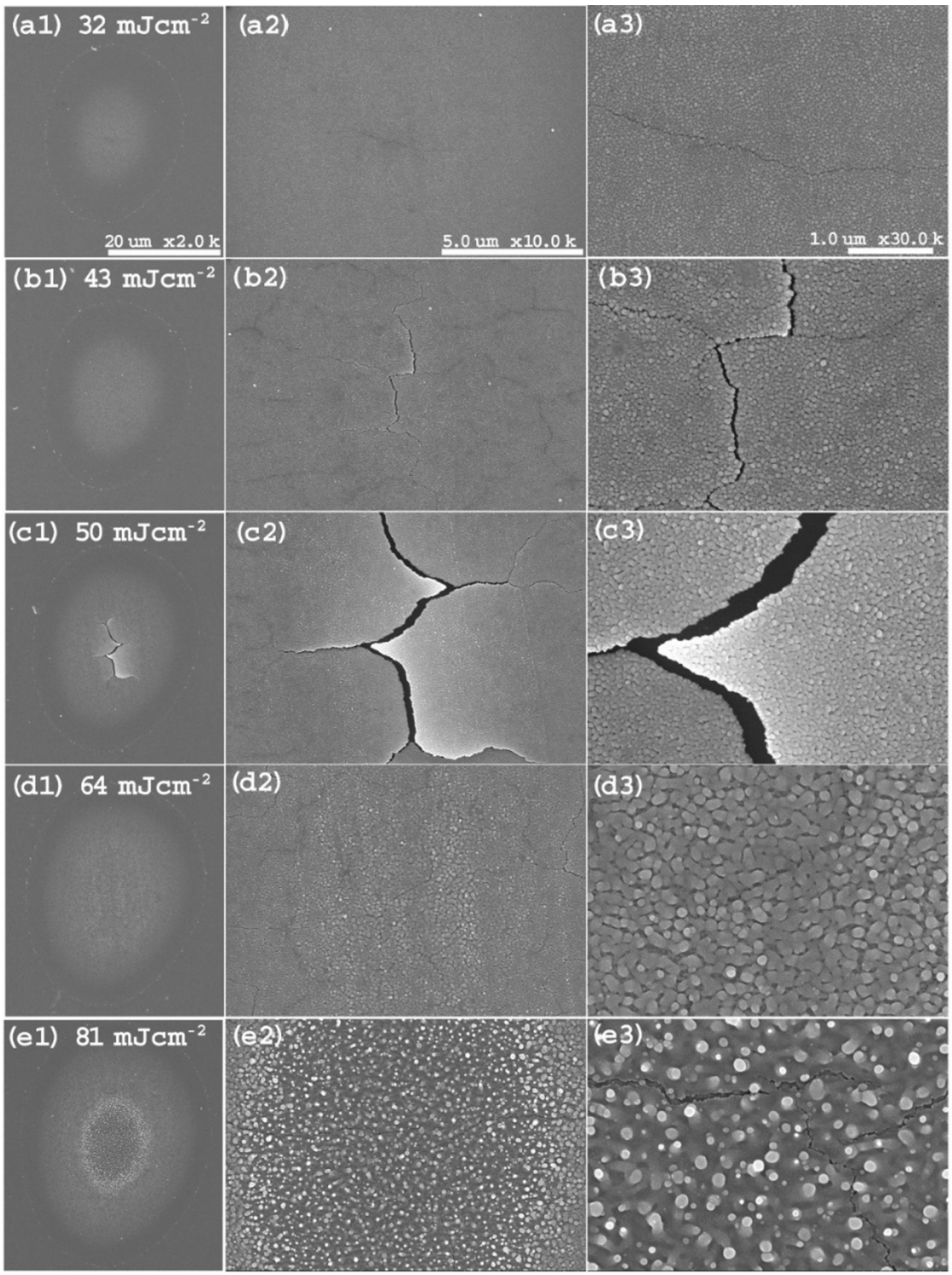

Fig. 8. SEM micrographs revealing the film response and surface nanostructuring of 80 nm thick Mo film in the different fluence regimes where two modes of ablation are evident. The scale bars in first row applies to all images in the same column.

minimum thermal conduction losses to the surroundings [18]. If the heat generated after laser energy absorption is confined within the laser irradiated volume during the onset of laser pulse and cannot escape via heat conduction, then thermal confinement is achieved. For this purpose, the laser pulse duration must be shorter than the thermal relaxation time (τ_{th}) as given below [29];

$$\tau_{th} = \frac{\delta^2}{4\chi}$$

here δ is optical penetration depth of the 515 nm laser (circa. 10.85 nm for Mo [30]) and χ is the thermal diffusivity (5.4×10^{-5} m^2s^{-1} [26]) of Mo. τ_{th} is calculated to be 0.54 ps which is greater than the laser pulse duration (500 fs) used in this study. This thermal confinement ($\tau_{th} >$ pulse duration) increases the temperature of the heated volume, and the rapid heating gives rise to a buildup of higher transient thermoelastic stresses which exceeds the film's fracture limit before any thermal expansion for stress relaxation occurs. The second important criteria for

stress assisted ablation is the condition for the generation of compressive stresses or normally referred to as stress confinement, as given by the following relation [31,32];

$$\tau_{ac} = \frac{\delta}{C_s}$$

where τ_{ac} is the acoustic relaxation time required to initiate the expansion of the heated lattice and C_s is the speed of sound in Mo (6.3×10^3 ms^{-1} [33]). For stress assisted ablation to occur, τ_{ac} must be greater than the laser pulse duration [32]. τ_{ac} is estimated to be 1.58 ps for Mo which is higher than the pulse width (500 fs). When the laser heating time is shorter than τ_{ac}, the heating takes place in a confined volume condition causing a buildup of stresses within the heated region since the heated area has not enough time to expand. This buildup up of compressive stresses act on the grain boundary interface and between the laser irradiated and non-irradiated areas and crack formation occurs [18]. The repeated application of laser heating and cooling following stress formation and relaxation cycles leads to the delamination of the film in a typical laser scanning configuration.

3.3.2. *Nanostructure formation and ablation assisted by nanoparticle emission -high fluence regime*

We observed the cracks formation and stress assisted ablation in 80 nm thick Mo film from 32 mJcm^{-2} to 50 mJcm^{-2} laser fluence, we marked this region as low fluence regime of ablation. No apparent melting of Mo and the underlying a-Si layer is seen in high resolution SEM images but instead an enhancement in the average particle size was observed. The laser fluence was raised higher to 64 mJcm^{-2} to study the variations on film morphology and on the ablation behavior. No apparent surface cracking is observed at this fluence but only the growth of nanostructures is evident (Fig. 8-d3). These nanostructures in the form of elongated ridges of width circa. 33 nm is pronounced and still composed of tiny nanosized particles. The density of these randomly organized ridges is higher at the center of the single pulse irradiated spot. Additionally, the formation of some nanoparticles at the tips of these nanostructures is also noticeable. When the fluence is increased to 84 mJcm^{-2}, the Mo film ablated in the form of nanoparticles from the surface (Fig. 8-e1). The ablation rate is higher at the center of the crater with a noticeable depletion in the density of the nanostructures (Fig. 8-e2). The size and the density of droplets (nanoparticles) at the top of nanostructures is increased as seen in Fig. 8-e3. The average size of these droplets is 25 nm $\pm$ 3 nm. Nano cracks appear at this stage and are only visible at high resolution.

4. Discussion

It is challenging to selectively process a high melting temperature Mo thin film on a substrate with a comparatively lower melting temperature since the heat generated can drastically damage the nearby components. The precise control and selection of laser parameters can enable processes from laser-induced crystallization to laser-induced ablation of the material. Mo thin films were treated at very low fluence (below ablation threshold) to avoid any damage/melting of the a-Si underneath as application of higher laser energies can fully melt the crystal lattice. The SEM results show that the melt free crystallization of Mo films results in an increase in the average grain size after scanning with femtosecond laser pulses. After absorbing the laser energy, the electronic excitation can change the electron density distribution in the solid resulting in modified interatomic forces. As a result, coherent atomic motion and the structural transition are produced on a very short time scale without electron–phonon coupling and are known as non-thermal phase transitions [34]. We propose that the enhanced crystallization after laser annealing occurs due to non-thermal solid-state diffusion of atoms in interstitial sites at a local scale of nanometers. The measurement of contact resistance before and after laser scanning resulted in a significant decrease of contact resistance revealing that crystallization also improves the adhesion and the flow of carrier transfer across the interface. Hall measurements provide strong evidence of improvement in the electrical properties with an overall enhanced carrier mobility after laser scanning. The mobility is primarily influenced by the continuity of the film structure and is related to the carrier's mean free path between collisions such as the scattering which takes place at the grain boundaries in the Mo film. An increase in mobility indicates an increase in the distance a carrier travels at the Fermi velocity before encountering a grain boundary. The carrier concentration of the Mo film is the number of free electrons present in the film and is observed to be less impacted by laser annealing. Therefore, we suggest that the relative scale of improvement in electronic mobilities as compared to electron concentration after laser annealing provides further evidence of enhanced grain sizes as a result of crystallization.

In ultrashort laser material ablation, the nature of the ablation mechanisms is strongly influenced by the combination of the thermodynamical, optical, and mechanical properties of the material as well as the laser processing parameters. Essentially, upon laser energy absorption, the corresponding thermodynamic and mechanical response of the material to the fast laser heating in a characteristic time domain determines the ablation mechanism. Using the green wavelength in the femtosecond time domain, it was possible to probe the different ablation mechanisms occurred in low and higher fluence range which were not resolved clearly in the past studies. Four film thicknesses such as 20 nm, 40 nm, 60 nm, and 80 nm are used for this study. At low fluence regime, nanostructures mediated partial ablation in the form of cavities (laser craters) was observed in 20 nm and 40 nm thin Mo films. No apparent surface cracking was observed on the film surface and upon increasing the fluence, the density of many local craters increases resulting in the formation of a bigger crater causing a complete delamination of the film from the center. In case of 60 nm and 80 nm thick Mo film, the ablation occurred due to mechanical effects in low fluence regime where the formation of tensile stresses and corresponding relaxation causes the delamination of Mo films. Crack formation is more evident at this stage and the ablation is purely due to stress assisted ablation mechanism. Upon increasing the fluence, no ablative effects are observed on the film surface and neither any cracking was appeared. When the laser fluence was raised to a significantly higher value, a complete removal of 60 nm film was observed from the center in the form of nanostructures and nanoparticle ejection. We marked this region as high fluence ablation regime for 60 nm thick Mo film. Whereas, in the case of 80 nm thick Mo film, no apparent cracking was realized on film surface with increasing laser fluence, and partial ablation was seen in the form of nanostructures formation and nanoparticle emission (Fig. 8-d3 & 8-e3). The ablation of materials in the form of nanoparticles at very high laser fluence could possibly be due to laser produced plasma plume. The laser-induced plasma plumes are a well-known source of the nanoparticles emission where the ablation efficiency is strongly related to the generation of the nanoparticles [35]. The studies on laser-induced plasma show that the two components in the emission spectrum of femtosecond laser ablated plasma plume of tungsten are observed referring to emission from the excited atoms at faster rate and a nanoparticle plume with a longer persistence time [36]. The atomization at early time of plasma plume formation is larger and the ablation efficiency is lower since the temperature near the target surface is higher, leading to more heat diffusion into the bulk. The heat diffusion into the bulk at low temperature is not capable of atomizing the deeper parts of the material and instead a mixture of gas and liquid (nanoparticles) emit out of the surface causing the ejection of the nanoparticles [35,36]. The onset of complete ablation occurred at the highest fluence of 84 mJcm^{-2} in 80 nm thick Mo film.

These key findings identify and exhibit the fluence regimes where one process appears, stops for some time and changes to another phenomenon with varying laser fluence, depending on the film thickness. In a recent study, the selective ablation of Mo from aluminum in a MAM multi-layered structure was conducted with IR femtosecond laser pulses. The origin of selective, clean ablation of Mo was perceived as an impact

of accumulated charge leading to multiple nanostructure formation accompanied by thermionic emission that leads to the fluence dependent electromechanical tensile stress causing the deformation at the interface [26]. The elongated nanostructures and the thermionic emission of electrons at higher laser energies were responsible for solid state clean delamination of Mo film from aluminum in the MAM heterostructure [26]. The stress assisted delamination and nanostructures enabled ablation along with nanoparticle emission from the crater are the two key ablation mechanism observed in our study using green femtosecond laser pulses. The emission of electrons plays an important role in material ablation and to incorporate electron emission, a further study with sophisticated measuring techniques should be carried out which is beyond the scope of this study. The in-depth analysis carried out in this study not only identifies the low fluence enhanced crystallization but also unveils the key regimes of ablation in high melting temperature Mo films of varying thickness without damaging the substrate providing a better understanding of the laser material interaction.

5. Conclusions

Femtosecond green laser pulses are used to crystallize and investigate the ablation behavior of high melting temperature Mo thin films. Carefully controlled, low fluence laser processing below the melting threshold enables the enhancement in the crystallinity of Mo films with varied thicknesses without impacting the substrate underneath. Laser enhanced crystallization not only enhances the average grain size, but it also improves the electrical properties with reducing the interface contact resistance. The reported direct low fluence efficient ultrashort-pulse annealing is promising to selectively crystallize high melting temperature Mo thin films in order to obtain high electrically conductive metal thin films for flexible electronics applications. The application of higher laser fluence reaching the ablation threshold causes the material ablation accompanied with nanostructure formation and nanoparticle emission. The mechanical fracture of films is observed in high thicknesses such as 60 nm and 80 nm thick Mo films where the film delaminates due to a tensile stress acting on the film surface. This study provides a deep understanding of the laser-induced processes from low fluence crystallization to high fluence ablation where the ultrashort laser pulses in the visible region can identify the different ablation mechanisms depending upon the film thickness and on the laser fluence. We believe that this study is relevant for better understanding and utilizing precise selective crystallization and clean ablation processes in high melting temperature materials for their improved applications in rapid, high speed and scalable industrial manufacturing.

Data Availability Statement.

Data is available on request from the corresponding author.

CRediT authorship contribution statement

Ayesha Sharif: Conceptualization, Data curation, Formal analysis, Investigation, Methodology, Software, Validation, Visualization, Writing – original draft, Writing – review & editing. **Nazar Farid:** Conceptualization, Data curation, Formal analysis, Investigation, Methodology, Software, Validation, Resources, Writing – review & editing. **Mingqing Wang:** Resources, Writing – review & editing. **Kwang-Leong Choy:** Resources, Writing – review & editing. **Gerard M. O'Connor:** Conceptualization, Validation, Resources, Project administration, Funding acquisition, Supervision, Writing – review & editing.

Declaration of Competing Interest

The authors declare that they have no known competing financial interests or personal relationships that could have appeared to influence the work reported in this paper.

Acknowledgments

This publication has emanated from research supported in part by a grant from Science Foundation Ireland under Grant number 16/RC/3872. For the purpose of Open Access, the author has applied public copyright license to any Author Accepted Manuscript version arising from this submission. Gerard M O'Connor's contribution and facilities are also supported by EU INTERREG project EAPA 384 2016 , "AtlanticKETMED". The authors gratefully acknowledge the SEM facility provided by The Centre for Microscopy and Imaging at and their support and assistance in this work.

References

[1] H.B. Michaelson, The work function of the elements and its periodicity, J. Appl. Phys. 48 (1977) 4729–4733.
[2] N. Farid, H. Wang, C. Li, X. Wu, H.Y. Oderji, H. Ding, G.-N. Luo, Effect of background gases at reduced pressures on the laser treated surface morphology, spectral emission and characteristics parameters of laser produced Mo plasmas, J. Nucl. Mater. 438 (2013) 183–189.
[3] C. Mitterer, T. Jörg, R. Franz, M. Mühlbacher, B. Sartory, F. Mendez-Martin, N. Schalk, Functional thin films for display and microelectronics applications, BHM Berg-und Hüttenmännische Monatshefte 160 (2015) 231–234.
[4] Y.-W. Yen, Y.-L. Kuo, J.-Y. Chen, C. Lee, C.-Y. Lee, Investigation of thermal stability of Mo thin-films as the buffer layer and various Cu metallization as interconnection materials for thin film transistor–liquid crystal display applications, Thin Solid Films 515 (2007) 7209–7216.
[5] J.A. Shields, P. Lipetzky, Molybdenum applications in the electronics market, JOM 52 (2000) 37–39.
[6] W. Hu, R. Peterson, Molybdenum as a contact material in zinc tin oxide thin film transistors, Appl. Phys. Lett. 104 (2014), 192105.
[7] D.-S. Han, Y.-J. Kang, J.-H. Park, H.-T. Jeon, J.-W. Park, Influence of molybdenum source/drain electrode contact resistance in amorphous zinc–tin-oxide (a-ZTO) thin film transistors, Mater. Res. Bull. 58 (2014) 174–177.
[8] E.G. Jeong, J.H. Kwon, K.S. Kang, S.Y. Jeong, K.C. Choi, A review of highly reliable flexible encapsulation technologies towards rollable and foldable OLEDs, Journal of Information Display 21 (2020) 19–32.
[9] N. Bansal, K. Pandey, K. Singh, B.C. Mohanty, Growth control of molybdenum thin films with simultaneously improved adhesion and conductivity via sputtering for thin film solar cell application, Vacuum 161 (2019) 347–352.
[10] P. Chelvanathan, S. Shahahmadi, F. Arith, K. Sobayel, M. Akharuzzaman, K. Sopian, F. Alharbi, N. Tabet, N. Amin, Effects of RF magnetron sputtering deposition process parameters on the properties of molybdenum thin films, Thin Solid Films 638 (2017) 213–219.
[11] X. Jia, Z. Lin, T.-C.-J. Yang, B. Puthen-Veettil, L. Wu, G. Conibeer, I. Perez-Wurfl, Post-sputtering heat treatments of molybdenum on silicon wafer, Applied Sciences 8 (2018) 1692.
[12] J. Dutta Majumdar, I. Manna, Laser material processing, Int. Mater. Rev. 56 (2011) 341–388.
[13] V.A. Khokhlov, Y.V. Petrov, N.A. Inogamov, K.P. Migdal, J. Winter, C. Aichele, S. Rapp, H.P. Huber, Dynamics of supported ultrathin molybdenum films driven by strong short laser impact, J. Phys. Conf. Ser. 1147 (2018) 012066, https://doi.org/10.1088/1742-6596/1147/1/012066.
[14] M. Domke, L. Nobile, S. Rapp, S. Eiselen, J. Sotrop, H.P. Huber, M. Schmidt, Understanding Thin Film Laser Ablation: The Role of the Effective Penetration Depth and the Film Thickness, Physics Procedia 56 (2014) 1007–1014.
[15] G. Heise, M. Englmaier, C. Hellwig, T. Kuznicki, S. Sarrach, H.P. Huber, Laser ablation of thin molybdenum films on transparent substrates at low fluences, Appl. Phys. A 102 (2011) 173–178.
[16] S. Zoppel, H. Huber, G.A. Reider, Selective ablation of thin Mo and TCO films with femtosecond laser pulses for structuring thin film solar cells, Appl. Phys. A 89 (2007) 161–163.
[17] J. Sotrop, A. Kersch, M. Domke, G. Heise, H.P. Huber, Numerical simulation of ultrafast expansion as the driving mechanism for confined laser ablation with ultrashort laser pulses, Appl. Phys. A 113 (2013) 397–411.
[18] N. Farid, H. Chan, D. Milne, A. Brunton, G.M. O'Connor, Stress assisted selective ablation of ITO thin film by picosecond laser, Appl. Surf. Sci. 427 (2018) 499–504.
[19] N. Farid, P. Dasgupta, G. O'Connor, Onset and evolution of laser induced periodic surface structures on indium tin oxide thin films for clean ablation using a repetitively pulsed picosecond laser at low fluence, J. Phys. D Appl. Phys. 51 (2018), 155104.
[20] N. Farid, A. Brunton, P. Rumsby, S. Monaghan, R. Duffy, P. Hurley, M. Wang, K.-L. Choy, G.M. O'Connor, Femtosecond Laser-Induced Crystallization of Amorphous Silicon Thin Films under a Thin Molybdenum Layer, ACS Appl. Mater. Interfaces 13 (31) (2021) 37797–37808.
[21] W.W. Duley, Laser Processing and Analysis of Materials, Springer, US, 2012.
[22] X. Wang, H. Yu, P. Li, Y. Zhang, Y. Wen, Y.e. Qiu, Z. Liu, YunPeng Li, L. Liu, Femtosecond laser-based processing methods and their applications in optical device manufacturing: A review, Opt. Laser Technol. 135 (2021) 106687, https://doi.org/10.1016/j.optlastec.2020.106687.
[23] E.G. Gamaly, Femtosecond Laser-Matter Interaction: Theory, Jenny Stanford Publishing, Experiments and Applications, 2011.

[24] S. Anisimov, B. Kapeliovich, T. Perelman, Electron emission from metal surfaces exposed to ultrashort laser pulses, Zh. Eksp. Teor. Fiz 66 (1974) 375–377.
[25] J. Chen, J. Beraun, Numerical study of ultrashort laser pulse interactions with metal films, Numerical Heat Transfer: Part A: Applications 40 (2001) 1–20.
[26] N. Farid, A. Sharif, P.D. Gupta, G.M. O'Connor, Selective laser ablation of molybdenum from aluminium in a multi-layered thin film system, Surf. Interfaces 26 (2021) 101438, https://doi.org/10.1016/j.surfin.2021.101438.
[27] J.M. Liu, Simple technique for measurements of pulsed Gaussian-beam spot sizes, Opt. Lett. 7 (5) (1982) 196, https://doi.org/10.1364/OL.7.000196.
[28] M.R. Querry, Optical constants of minerals and other materials from the millimeter to the ultraviolet, Chemical Research, Development & Engineering Center, US Army Armament … (1987).
[29] J. Winter, M. Spellauge, J. Hermann, C. Eulenkamp, H.P. Huber, M. Schmidt, Ultrashort single-pulse laser ablation of stainless steel, aluminium, copper and its dependence on the pulse duration, Opt. Express 29 (10) (2021) 14561, https://doi.org/10.1364/OE.421097.
[30] E.D. Palik, Handbook of optical constants of solids, Academic press (1998).
[31] G. Paltauf, P.E. Dyer, Photomechanical processes and effects in ablation, Chem. Rev. 103 (2003) 487–518.
[32] L.V. Zhigilei, Z. Lin, D.S. Ivanov, Atomistic modeling of short pulse laser ablation of metals: connections between melting, spallation, and phase explosion, The Journal of Physical Chemistry C 113 (2009) 11892–11906.
[33] T.S. Duffy, T.J. Ahrens, Dynamic response of molybdenum shock compressed at 1400 C, J. Appl. Phys. 76 (1994) 835–842.
[34] Y. Giret, S.L. Daraszewicz, D.M. Duffy, A.L. Shluger, K. Tanimura, Nonthermal solid-to-solid phase transitions in tungsten, Physical Review B 90 (2014), 094103.
[35] S. Noël, J. Hermann, T. Itina, Investigation of nanoparticle generation during femtosecond laser ablation of metals, Appl. Surf. Sci. 253 (2007) 6310–6315.
[36] S. Harilal, N. Farid, A. Hassanein, V. Kozhevin, Dynamics of femtosecond laser produced tungsten nanoparticle plumes, J. Appl. Phys. 114 (2013), 203302.